Norwegian Meteorological Institute

METreport

No. 09/2022
ISSN 2387-4201
Meteorology

All-sky assimilation of MHS humidity microwave radiances in Arome-Arctic

ALERTNESS project deliverable

Roohollah Azad, Roger Randriamampianina

Title All-sky assimilation of humidity microwave radiances in Arome-Arctic	**Date** 20 May 2022
Section Meteorology	**Report no.** No. 09/2022
Author(s) Roohollah Azad , Roger Randriamampianina	**Classification** ● Free ○ Restricted
Client(s) Norwegian research council	**Client's reference** Project number 280573 ‘Advanced models and weather prediction in the Arctic: enhanced capacity from observations and polar process representations (ALERTNESS)

Abstract

This report describes the work done as part of the ALERTNESS project to introduce and implement the ECMWF all-sky radiance assimilation method in the regional NWP model Harmonie-Arome and over the Arome-Arctic domain. The implementation is performed in cy46 and focusing on the humidity sensitive microwave radiances from MHS sensors on NOAA and METOP satellites. To activate the all-sky observation operator RTTOV-SCATT the hydrometeor variables from Harmonie-Arome forecasts are added in the interface as well as the cloud fraction to calculate the contributions from clear and cloudy brightness temperature. The model hydrometeor variables are needed in the forward observation operator to derive the model counterpart of the observations. Since the hydrometeors are not in the control variables they are set to zero in the minimization. As a first step, the all-sky observations over land from all channels and everywhere for channel 5 is blacklisted to avoid the emissivity issues with RTTOV-SCATT implementation. The first trials for a one week period showed promising results for the statistics of first guess departures, analysis departures, and analysis increments. Finally, the impact of all-sky observation on upper-air forecasts is shown to be neutral on the verifications against radiosonde observations, although a reduction in the wind speed forecast error is observed when assimilating all-sky observations on top of conventional observations.

Keywords

regional data assimilation, microwave radiance, all-sky

Disciplinary signature

Responsible signature

Abstract

This report describes the work done as part of the ALERTNESS project to introduce and implement the ECMWF all-sky radiance assimilation method in the regional NWP model Harmonie-Arome and over the Arome-Arctic domain. The implementation is performed in cy46 and focusing on the humidity sensitive microwave radiances from MHS sensors on NOAA and METOP satellites. To activate the all-sky observation operator RTTOV-SCATT the hydrometeor variables from Harmonie-Arome forecasts are added in the interface as well as the cloud fraction to calculate the contributions from clear and cloudy brightness temperature. The model hydrometeor variables are needed in the forward observation operator to derive the model counterpart of the observations. Since the hydrometeors are not in the control variables they are set to zero in the minimization. As a first step, the all-sky observations over land from all channels and everywhere for channel 5 is blacklisted to avoid the emissivity issues with RTTOV-SCATT implementation. The first trials for a one week period showed promising results for the statistics of first guess departures, analysis departures, and analysis increments. Finally, the impact of all-sky observation on upper-air forecasts is shown to be neutral on the verifications against radiosonde observations, although a reduction in the wind speed forecast error is observed when assimilating all-sky observations on top of conventional observations.

Table of contents

1 Introduction

The numerical weather prediction (NWP) is an initial value problem where one needs to provide the initial state from which the model integration can start and the state of the atmosphere can evolve. The more accurate the estimate of the initial values, the better the quality of the forecasts. Data assimilation is the process of combining observations and short-range forecasts to obtain the initial condition of the atmospheric state. This technique consists of two parts, the background and the observations. Considering the latter, there are insufficient observations at any time to determine the state of the atmosphere. Therefore, satellite observations are of huge importance in NWP not only for their broad coverage but also for the measurements from the entire depth of the atmosphere everywhere over the globe. However, radiance measurements in the cloudy and rainy regions are rejected in data assimilation in our regional NWP system and this report describes the steps taken toward assimilation of cloudy and rainy microwave radiances from MHS sensors on NOAA and METOP satellites.

Satellite measurements are referred to as remotely sensed observations mainly because the atmospheric quantities are not measured directly. In fact, satellites measure the radiation emitted by Earth's surface and the surrounding atmosphere. Retrieval or physical models must be utilised to relate the satellite radiation measurements to the geophysical parameters used in NWP such as temperature, humidity, and winds. Traditionally, the geophysical parameters have been first retrieved from the satellite data and assimilated into the NWP models. In this approach, first the satellite retrievals were provided by the satellite data producers, then assimilated in the NWP system. In the direct radiance assimilation this processing step is carried out within the NWP system and therefore suits better for operational applications. Furthermore, in

the direct radiance assimilation the complicated error contamination in different retrieval processes can be avoided, which means that less source of error remains to be handled. In other words, the observational error statistics are better justified in direct assimilation than the retrieval assimilation (*McNally et al.,* 2000). The direct assimilation approach requires an observation operator to transform model variables into radiances. For satellite radiances, the linkage between forecast model state variables and observed radiances is defined mathematically by a forward radiative transfer model (RTTOV - *Saunders et al.,* 2018) which calculates radiance from model vertical profiles.

Satellite humidity observations have in recent years shown to have considerable impact on weather forecasts (e.g.: *Randriamampianina et al.,* 2021*, Lawrence et al.,* 2019). This is because free-troposphere humidity features are principally driven by winds. Such inference is of course more straightforward for satellite temperature observations where the temperature field would yield wind information through the geostrophic balance in the background error covariances (Smagorinsky et al., 1970). For both satellite temperature and humidity measurements, the presence of thick clouds and precipitating clouds are challenging. The first observation operators used for satellite radiance assimilation are designed for clear and thin cloudy radiances and the observations from thick cloudy and rainy radiances are removed. To take into account for cloudy and rainy radiances the all-sky assimilation was developed at ECMWF (Geer et al., 2014). Microwave humidity sounding observations are ideal for all-sky assimilation since they show relatively smooth and linear response to water vapour, cloud and precipitation (*Bauer et al.,* 2010). One important step in the use of all-sky observation operators in data assimilation is to accurately simulate scattering effect from the frozen particles at the high microwave frequencies used for humidity sounding (*Geer and Baordo*, 2014).

In this short report, we present the work and results from the implementation of ECMWF's all-sky method in our regional NWP model. Such implementation is possible since our regional NWP model shares to a large extent the same codes with ECMWF Integrated Forecasting System (IFS). In section 2 we describe the regional NWP model and the data assimilation method. Section 3 describes the all-sky data assimilation approach in IFS and how this is implemented in our regional model. Section 4 describes the technical implementation of the ECMWF's all-sky method in a version of our suitable local NWP system for all-sky assimilation (CY46). The first data assimilation results and a one week period impact study is described in section 5 and 6. Finally in section 7 we summarise the work and the main lessons learned for a future operational all-sky assimilation in our regional NWP system.

2 Harmonie-Arome

The numerical weather prediction system used at MET Norway is based on the Harmonie-Arome (HIRLAM-ALADIN Regional Mesoscale Operational NWP In the Europe Application of Research to Operations at Mesoscale) model (*Bengtsson et al,* 2017). The version used in this study is the cycle 46 (CY46) of a branch of the Harmonie-Arome and is used for a geographical domain covering a large part of the European Arctic called Arome-Arctic (see *Muller et al*, 2017). This model has a horizontal resolution of 2.5 km where the horizontal grid (739 × 949 grid points) is defined by a Lambert projection with the centre at 63°N and 15°E. In the vertical, sixty five levels are used by a general pressure based and terrain following vertical coordinate, with the model top at 10 hPa and the lowest level at around 12 m. The model is forced by the ECMWF model, which has approximately 9 km horizontal resolution and 137 vertical levels, at the lateral and upper boundaries. In order to simulate the operational runs, ECMWF lateral boundaries used in this study are at least 6 hours old.

Harmonie-Arome uses a nonhydrostatic (NH) dynamical core and is based on the fully compressible Euler equations. These equations are discretized in time and space using a two-time-level, semi-Implicit, semi-Lagrangian advection scheme on an A grid. We refer readers to Seity et al. (2011) and Bengtsson et al. (2017) for a complete description of the model physics. However, several modifications are included for the high latitudes to reduce the 2m temperature bias in winter and to improve the low-level cloudiness (*Muller et al*, 2017). It should be mentioned that deep convection is explicitly represented by the model's nonhydrostatic dynamics at 2.5-km resolution and therefore there is no parameterization of deep convection in the model. Meanwhile, shallow convection is not resolved at this resolution and needs to be parameterized. Achievement of more accurate performance of the Harmonie-Arome especially for the surface parameters is realised through an offline coupling with the SURFEX (Surface Externalisée) model (Masson et al., 2013). The reader is referred to Bengtsson et al. (2017) and Muller et al. (2017) for more details regarding the dynamic, physic and surface part of the model.

The upper-air data assimilation in the Harmonie-Arome model is a 3 dimensional variational (3DVAR) assimilation scheme based on a three-hourly rapid update cycle to analyse wind, temperature, specific humidity, and surface pressure fields (*Fischer et al.*, 2005, *Randriamampianina et al.,* 2019). The background-error covariances (B) are calculated from ensemble global perturbed analyses downloaded to the regional domain and projected to a 6-hour forecast. The balances are purely statistical as they are estimated through multivariate linear regression (*Berre,* 2000).
The cost function **J** to be minimised is shown below which consists of two parts in the right hand side.

$$J(\mathbf{x}) = (\mathbf{x}-\mathbf{x}_b)^T\mathbf{B}^{-1}(\mathbf{x}-\mathbf{x}_b) + (\mathbf{y}-H(M(\mathbf{x})))^T\mathbf{R}^{-1}(\mathbf{y}-H(M(\mathbf{x})))$$

The control variables **x** are temperature, humidity, wind, and surface pressure. In fact the wind part is formulated through the divergence and vorticity. The first part in the right hand side of the cost function is the background term where **B** is the background error covariance matrix. The second term in the observation term where ***H*** is the observation operator and **R** is the observation error covariance matrix. For the clear-sky radiance assimilation, ***H*** is the RTTOV while for the all-sky radiance assimilation *H* is RTTOV-SCATT. In fact, we want to activate this observation operator in the Harmonie-Arome.

3 All-sky radiance assimilation

3.1 Observation operator

The radiative transfor model RTTOV-SCATT used as observation operator for the all-sky radiance assimilation is a very fast radiative transfer model for simulating satellite radiances (*Eyre*, 1991; *Saunders et al*., 2018). The RTTOV-SCATT computes the top of atmosphere radiances in each of the channels of the sensor being simulated using atmospheric profile of temperature, humidity, trace gases, aerosols and hydrometeors, also a viewing geometry and surface parameters. In the clear-sky

radiance assimilation the RTTOV will use all the parameters above except for the hydrometeors (Figure 1). The radiative transfer equation is solved using the delta-Eddington approximation (*Joseph et al.*, 1976). Lookup tables are used to take the bulk optical properties of hydrometeors, where the optical properties of cloud water, cloud ice and rain hydrometeors are generated using Mie theory (*Bauer*, 2001) while the optical properties of snow hydrometeors from discrete dipole calculations (*Geer and Baordo*, 2014). The all-sky brightness temperature is computed as the weighted average of the brightness temperature from two independent subcolumns, one cloudy and one clear shown below

$$\mathbf{TB_{all\text{-}sky} = (1\text{-}C_{total}) \times TB_{clear\text{-}sky} + C_{total} \times TB_{cloudy}}$$

where C is cloud fraction. In fact, this is a weighting performed according to the effective cloud fraction which accounts for the effects of subgrid variability in cloud and precipitation (*Geer et al.* 2009).

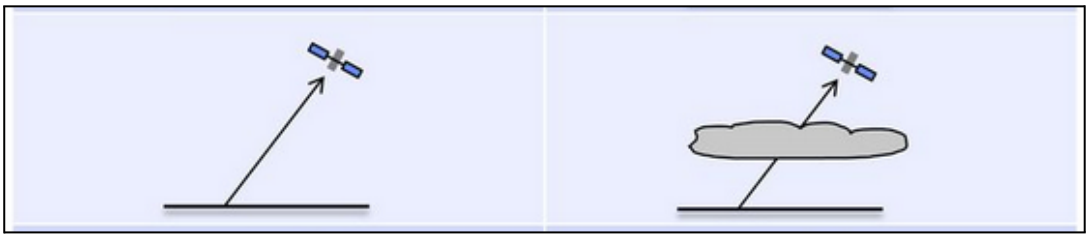

Figure 1.- all-sky radiance concept (right) against the currently operational clear-sky approach (left) where in the all-sky the rainy and thick cloudy radiances are also taken into account.

In the data assimilation, the radiance observations can be assimilated in two different ways. In the direct assimilation the observation operators like RTTOV or RTTOV-SCATT are used to calculate the brightness temperature which then will be used directly in the cost function. For indirect assimilation the observation operators are used to retrieve humidity and temperature which will then be put into the cost function. A method called BAYRAD developed at Meteo France uses model temperature and humidity in the RTTOV-SCATT to simulate all-sky radiances in a so-called indirect all-sky assimilation (*Guerbette et al.*, 2016) similar to the Bayesian retrieval used to assimilate the radar reflectivity observations. To our knowledge, however, the all-sky method developed at ECMWF is used directly for the first time in a limited area model in Europe in this project.

3.2 Observation error

There are a few differences between using RTTOV and RTTOV-SCAT in radiance assimilation which will be explained here. One of the differences is that in the clear-sky assimilation the observation errors are defined as constant values and the

dominant source of error is instrument noise and radiative transfer inaccuracies. For all-sky the dominant source of error is representivity because the model can not simulate cloud and precipitation correctly with inaccuracies in both intensity and location. In IFS these errors are treated as observation errors and therefore the thinning or superobing of MHS observation would be required. The main difference compared to clear-sky comes to the picture when we apply an observation error model. This model inflates observation errors as a function of cloud amount which is an average amount of cloud or precipitation in the model and observations (*Baordo et al.*, 2012).

3.3 Quality control

We use the same blacklisting strategy for both clear-sky and all-sky but the thinning is done differently which will be explained in section 4.5. The main quality control procedure is the first guess check where the observations are rejected when they are far from the first guess in magnitude. Since the first guess is a model 3h forecast then we need to take into account that the cloud and precipitation intensity and location could be very different from the observations. Also for the sake of safety in our first try to assimilate all-sky we have decided to not assimilate observations over land.

3.4 Bias correction

The procedure to remove biases in all-sky is similar to clear-sky where variational bias correction is used to adaptively remove biases (*Dee*, 2004; *Auligné et al.*, 2007). It is worth to mention that no attempt is made in VarBC to correct cloud and precipitation related biases since these are addressed through the improvements in the RTTOV-SCATT or the forecast model, or the quality control applied to remove biassed observations. At this stage, our focus was on the implementation of the all-sky assimilation approach. Although, the presented results in this report shows a stable behaviour of the solution applied for assimilation of clear-sky radiance in VarBC, we will account for IFS solution concerning the update of the coefficients (use the mode of the first-guess departure instead of starting from zero in our clear-sky case) in later tests.

3.5 Moist physics

In the all-sky paradigm the cloudy and precipitating radiances are assimilated. This means that the hydrometeors in the model are used to calculate the model counterpart of the all-weather observations. On the other hand, the hydrometeors, both clouds and precipitation, are a 3 hourly Arome forecast. The quality of the forecast especially with regards to the intensity and location of precipitation is crucial to successfully assimilate rainy observations. Otherwise, observations are rejected in the quality control or given less weight because the observed and the forecast precipitations do

not match. There are two liquid and two frozen hydrometeor types which are provided by Harmonie-Arome to RTTOV-SCATT. For the cloud, the cloud liquid water and cloud ice water, and for the precipitation, the rain and snow are included while the graupel is not considered in this study because the interface version of IFS we use does not use it. Having the hydrometeors present in the minimization for the trajectory causes problems to the 3DVAR. Since the hydrometeors are not included in the control variable, we keep all TL and AD arrays of hydrometeors to zero to protect the system.

4 Implementation

4.1 Bator – conversion from BUFR to ODB

The interface between the observations and the data assimilation part of the code is provided by Bator. In this part of the code, the observations inside the domain which are in bufr format are read and then converted into a data format called ODB (Observation DataBase) which is the input to the data assimilation system. For cycle 46, preliminary works began with modifications in the Bator scripts and codes to prepare the interface firstly for conventional and clear-sky radiances. For the all-sky observations, a new observation type with OBSTYPE=16 was then introduced. To do this, we made the choice to switch off the clear-sky (radiance observation type with OBSTYPE=7) avoiding the use of both clear-sky and all-sky at the same time for each implemented instrument. Also, the all-sky has a different type of code type used later in the data assimilation system which is CODTYPE=215 in contrast to the clear-sky which is CODTYPE=210. Figure 2 shows that the same number of observations are provided by Bator for clear-sky and all-sky observations. This is because we want to give the same amount of observations to the all-sky observation operator.

LAMFLAG: OBSERVATION LISTING

OBSTYPE	STATUS	TOTAL	SELECTED
SYNOP	T	0	0
AIREP	T	0	0
SATOB	F	0	0
DRIBU	T	0	0
TEMP	T	0	0
PILOT	T	0	0
SATEM	T	371970	5682
PAOB	F	0	0
SCATT	F	0	0
SLIMB	F	0	0
OBT11	F	0	0
OBT12	F	0	0
RADAR	F	0	0
OBT14	F	0	0
LIDAR	F	0	0

LAMFLAG: OBSERVATION LISTING

OBSTYPE	STATUS	TOTAL	SELECTED
SYNOP	T	0	0
AIREP	T	0	0
SATOB	F	0	0
DRIBU	T	0	0
TEMP	T	0	0
PILOT	T	0	0
SATEM	F	0	0
PAOB	F	0	0
SCATT	F	0	0
SLIMB	F	0	0
OBT11	F	0	0
OBT12	F	0	0
RADAR	F	0	0
OBT14	F	0	0
LIDAR	F	0	0
ALLSKY	T	371970	5682

Figure 2. Number of observations in the clear- and all-sky conditions for one data assimilation cycle. Note that clear-sky and all-sky share the same number of observations at this stage of the data assimilation.

4.2 Screening

In this stage of the assimilation process, all observations from the Bator stage are quality controlled. The main part consists of comparing the observations with the first-guess (a 3h model forecast at observation location) in the observation space. Here, one needs to use the forward and nonlinear observation operator (RTTOV-SCAT) to calculate the model brightness temperature. In cy46, one needs a new version of the RTTOV coefficients and new observation error files for each satellite. In fact, the RTTOV-SCAT observation operator is called for the first time during the screening. To activate the forward observation operator several parts of the code needed to be updated. The main modification to have all-sky also for limited area models is in the GOM part of the code. We made modifications in the interface between the GOM part and the RTTOV-SCAT observation operator to include the cloud variables as well as rain and snow. One difference between Arome and IFS is the units for cloud, rain and snow inputs. In IFS codes these variables need to be converted from density to mixing ratio but in Arome these variables are already mixing ratios and no conversion is needed.
The observation error R is different for the clear-sky and all-sky with the latter using the precalculated error files from the operational IFS all-sky assimilation. The observation operators consist of two parts as $H=H_vH_h$ where the horizontal part (H_h) is calculated first. To start with, model counterparts of each observation are structured in GOM arrays around each observation. The IFS code needs on top of main model outputs like wind, temperature, and humidity also diagnostic moist physics. Note that at Meteo France, an all-sky solution using the Beysian approach, similar to the one used for radar reflectivity assimilation and called BYRAD, was successfully implemented (*Guerbette et al.*, 2016). When comparing what has been done for BAYRAD, we see that instead of IFS physics parameters in Arome other parameters are filled in GOM. These are snow water content (s), rain water content (R), cloud liquid water content (L), cloud ice content (I), and cloud fraction (A). Also the RTTOV-SCATT requires the precipitation fraction which is initialised to zero before the call to the RTTOV-SCATT operator.

4.3 Minimization

We started to make similar modifications we made for the forward part of the code aslo in the TL and AD parts. One main issue is that the hydrometeors are not yet in the control variable, therefore all TL and AD arrays of hydrometeors should be kept to zero to protect the assimilation system. This is shown in the figure 3 where the GOM variables are filled with corresponding values in the cost function calculation but are set to zero in the minimization stage. It should be mentioned here that these

hydrometeor variables are yet to be included in the control variables for a complete all-sky assimilation and until then the impact of assimilating cloudy and rainy radiances will be through the humidity adjustments, very similar to the BAYRAD method in Arome and radar reflectivity assimilation.

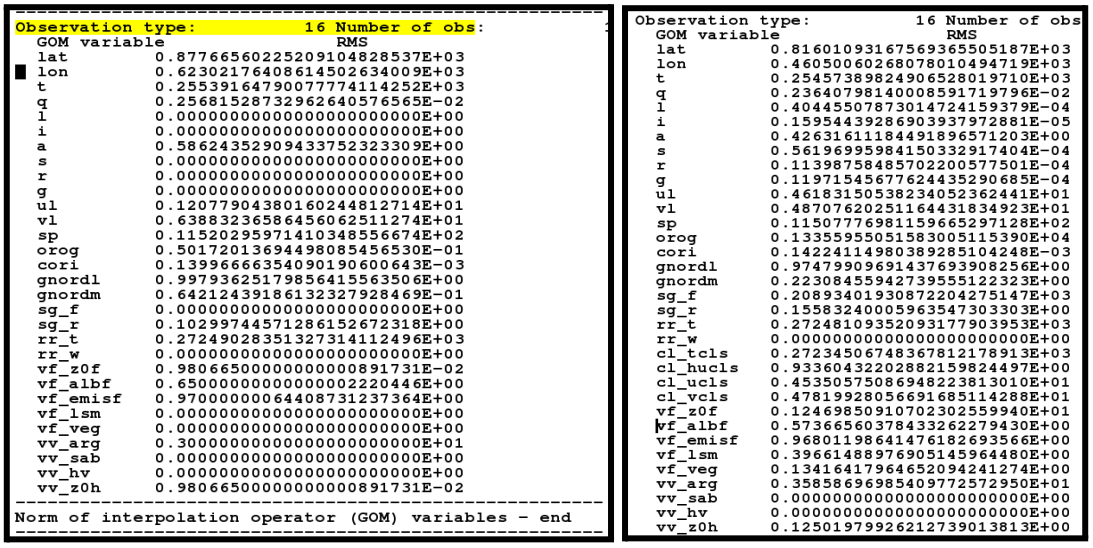

```
Observation type:          16 Number of obs:
  GOM variable                    RMS
  lat          0.87766560225209104828537E+03
  lon          0.62302176408614502634009E+03
  t            0.25539164790077774114252E+03
  q            0.25681528732962640576565E-02
  l            0.00000000000000000000000E+00
  i            0.00000000000000000000000E+00
  a            0.58624352909433752323309E+00
  s            0.00000000000000000000000E+00
  r            0.00000000000000000000000E+00
  g            0.00000000000000000000000E+00
  ul           0.12077904380160244812714E+01
  vl           0.63883236586456062511274E+01
  sp           0.11520295971410348556674E+02
  orog         0.50172013694498085456530E-01
  cori         0.13996666354090190600643E-03
  gnordl       0.99793625179856415563506E+00
  gnordm       0.64212439186132327928469E-01
  sg_f         0.00000000000000000000000E+00
  sg_r         0.10299744571286152672318E+00
  rr_t         0.27249028351327314112496E+03
  rr_w         0.00000000000000000000000E+00
  vf_z0f       0.98066500000000000891731E-02
  vf_albf      0.65000000000000002220446E+00
  vf_emisf     0.97000000064408731237364E+00
  vf_lsm       0.00000000000000000000000E+00
  vf_veg       0.00000000000000000000000E+00
  vv_arg       0.30000000000000000000000E+01
  vv_sab       0.00000000000000000000000E+00
  vv_hv        0.00000000000000000000000E+00
  vv_z0h       0.98066500000000000891731E-02
Norm of interpolation operator (GOM) variables - end
```

```
Observation type:          16 Number of obs
  GOM variable                    RMS
  lat          0.81601093167569365505187E+03
  lon          0.46050060268078010494719E+03
  t            0.25457389824906528019710E+03
  q            0.23640798140008591719796E-02
  l            0.40445507873014724159379E-04
  i            0.15954439286903937972881E-05
  a            0.42631611184491896571203E+00
  s            0.56196995984150332917404E-04
  r            0.11398758485702200577501E-04
  g            0.11971545677624435290685E-04
  ul           0.46183150538234052362441E+01
  vl           0.48707620251164431834923E+01
  sp           0.11507776981159665297128E+02
  orog         0.13355955051583005115390E+04
  cori         0.14224114980389285104248E-03
  gnordl       0.97479909691437693908256E+00
  gnordm       0.22308455942739555122323E+00
  sg_f         0.20893401930872204275147E+03
  sg_r         0.15583240005963547303303E+00
  rr_t         0.27248109352093177903953E+03
  rr_w         0.00000000000000000000000E+00
  cl_tcls      0.27234506748367812178913E+03
  cl_hucls     0.93360432202882159824497E+00
  cl_ucls      0.45350575086948223813010E+01
  cl_vcls      0.47819928056691685114288E+01
  vf_z0f       0.12469850910702302559940E+01
  vf_albf      0.57366560378433262279430E+00
  vf_emisf     0.96801198641476182693566E+00
  vf_lsm       0.39661488976905145964480E+00
  vf_veg       0.13416417964652094241274E+00
  vv_arg       0.35858696985409772572950E+01
  vv_sab       0.00000000000000000000000E+00
  vv_hv        0.00000000000000000000000E+00
  vv_z0h       0.12501979926212739013813E+00
```

Figure 3. Printout of GOM variables in the screening (right) and the minimization (left) stages. Notice that in the screening the physics variables are positive numbers but in the minimization cloud liquid (l), cloud ice (i), snow (s), rain (r), graupel (g) are forced to be zero.

4.4 Blacklisting

To remove observations of bad quality even before screening and minimization we used a local version of bator_liste structure very similar to the clear-sky. Another local blacklisting is implemented in screening. The difference is that in the all-sky assimilation also observations over land are blacklisted as well as observations in channel 5. For the Arome-Arctic domain which covers mostly sea area the former blacklisting will not make huge changes in the number of observations available for assimilation.

4.5 Thinning

At ECMWF a special approach is used to remove the observations very close to each other. The method is in fact a superobbing technique which will keep the pattern of observation locations even after thinning. Observations are put onto a Gaussian grid corresponding to T799 resolution, and the maximum distance from grid point is set to 100 km. A further thinning of the data is keeping only observations associated with grid points at every nth longitude and mth latitude. An example of thinning with different m and n is shown in figure 4. The optimal thinning is achieved by changing

the m,n so that the observations are not too close to each other, a distance which is set to 80km in the clear-sky assimilation.

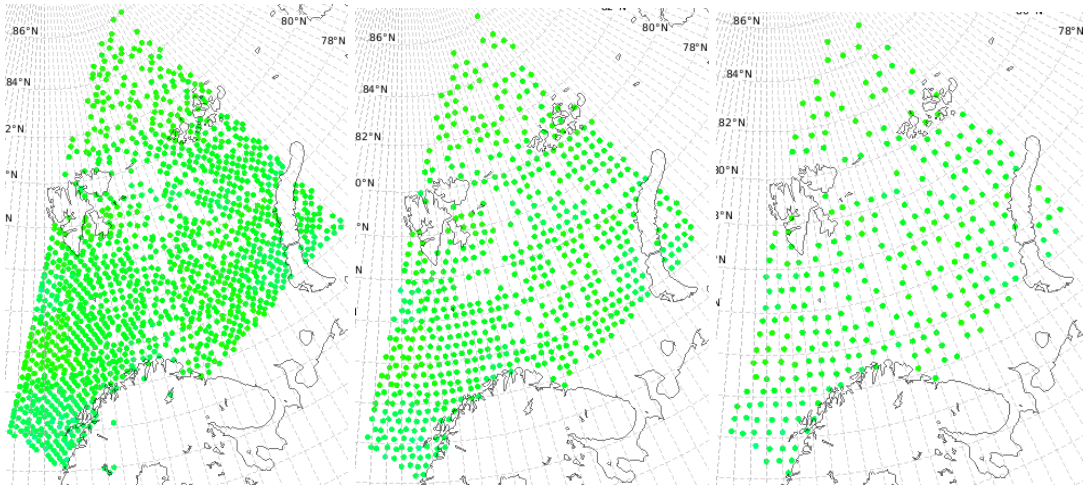

Figure 4. all-sky thinning using ECMWF method with n=1, m=-2 (left), n=2, m=2 (middel), and n=3, m=3 (right) showing the observations used in minimization.

5 preliminary statistics

We started testing the all-sky assimilation for only one assimilation cycle at 06 UTC 3rd October 2020 for a smaller domain over Denmark. The purpose of this testing was to make sure the all-sky data assimilation as whole is working properly and the assimilated all-weather radianced show the statistical characteristics to some extent similar to the clear-sky radiance assimilation. It should be mentioned that as for all parts of this work package we focused only on humidity sensitive microwave radiances from MHS sensors on NOAA and METOP.

5.1 Observation, background and analysis statistics

The first results are the observation minus background (o-b) histograms for clear-sky and all-sky assimilated for one cycle to show whether the all-sky assimilation is biassed. Figure 5 shows the o-b for observations in the screening stage for the all-sky

and clear-sky mhs assimilation where the first guess (b) is the same for both cases. The mean differences indicate that the model interpolated to observation location (b) in clear-sky and all-sky are not much different from each other. For the standard deviations there is a slightly larger variability in the all-sky though.

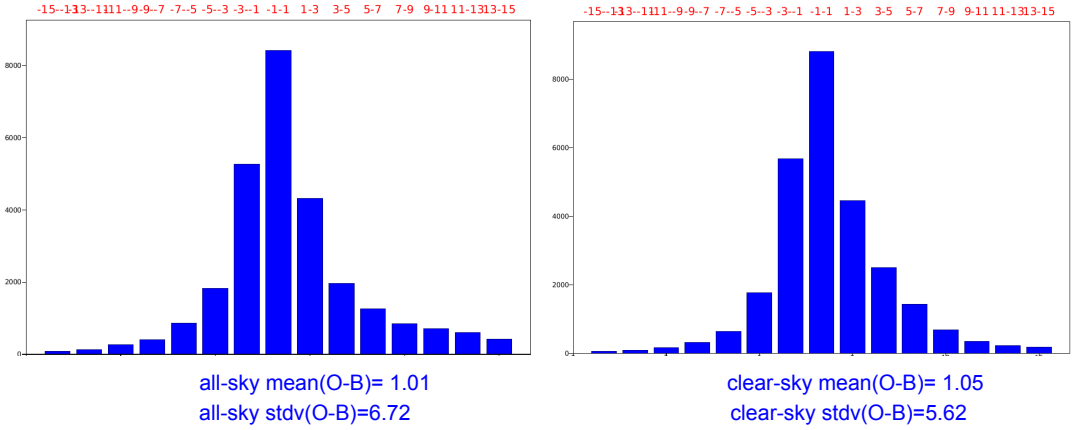

Figure 5. Histogram of observation minus background for all-sky (left) and clear-sky (right) assimilation in screening at 2020100306. The mean and standard deviations are shown with the blue texts.

In the vertical shown in figure 6 the o-b for the clear-sky and all-sky are similar to each other than that of the standard deviations which are slightly larger at all levels in the all-sky. These results confirm that the all-sky observation operator produces model brightness temperatures which are very close to the clear-sky when most of the domain is cloud-free. In the minimization stage, the observation minus analysis (o-a) are available and figure 6 shows that both the mean and standard deviations of o-a values are smaller than o-b values confirming that the data assimilation is working properly for the all-sky.

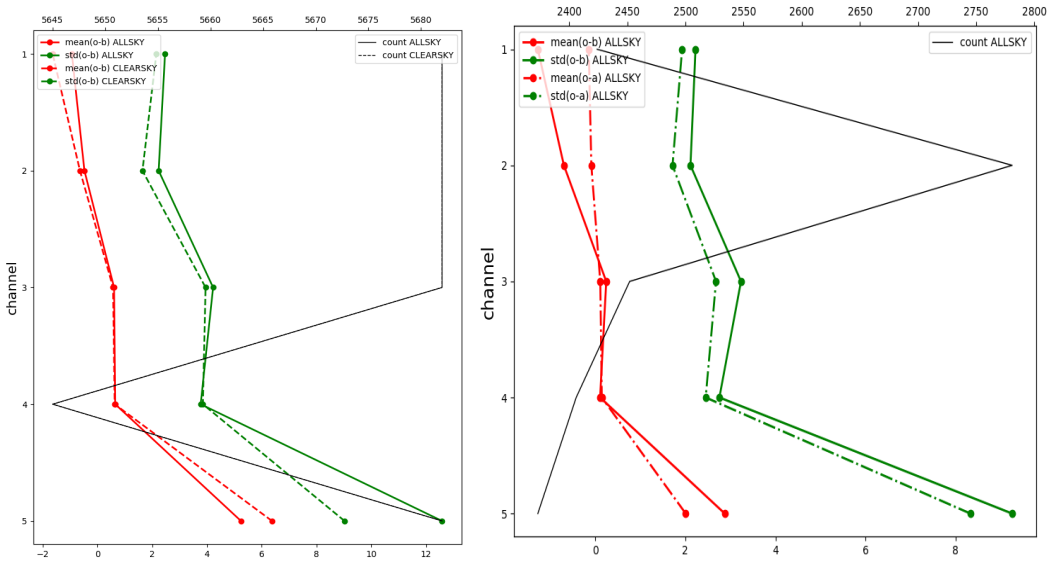

Figure 6 the mean (red) and standard deviations (green) of o-b for the all-sky (solid) and clear-sky assimilation (dashed) to the left, and the mean (red) and standard deviations (green) of o-b (solid) and o-a (dashed) in the minimization for all-sky assimilation to the right at 06 UTC 3rd October 2020.

5.2 Tb distribution in screening

After having successfully assimilated all-sky MHS radiances in one cycle, we examined the distribution of model brightness temperature and compared with the observations and the clear-sky counterpart. Figure 7 shows the distribution for all five channels where the three higher level channels will be used in the minimization. It is interesting to mention that for channel 3 the occurrence of lower temperatures in the observations fits well with the all-sky Tb while it is overrepresented in the clear-sky Tb.

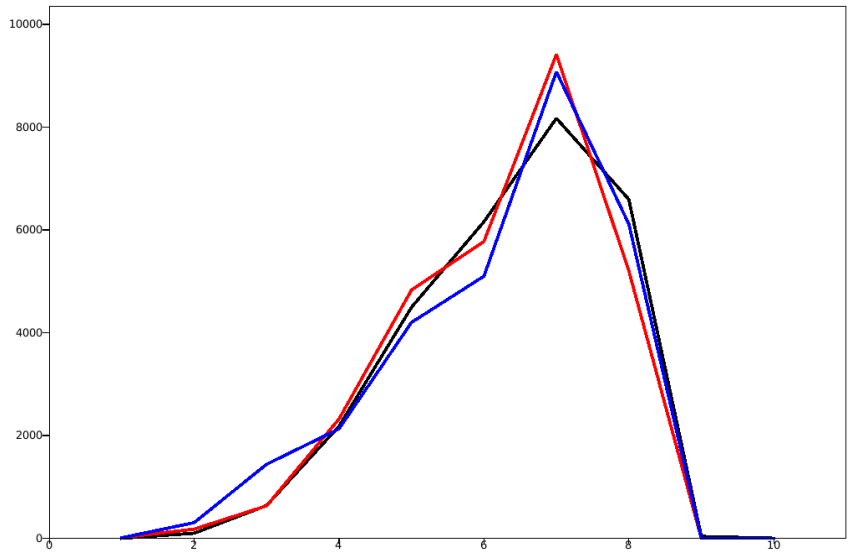

Figure 7. The distribution of observed (blak), all-sky (red) and clear-sky (blue) brightness temperature for all five channels from the MHS sensor at 06 UTC 3rd October 2020. The horizontal axis shows the Tb values divided by 100.

5.3 Rainy and cloudy observations

In the clear-sky assimilation all rainy and thick cloudy radiances are blacklisted during the screening while in the all-sky assimilation we have all-weather radiances in the screening and minimization. Figure 8 shows the geographical distribution of observations and the observations minus analysis (o-a) values. Comparing with the cloud and precipitation field, one can find out that in the rainy areas especially to the west of western coast of Norway the observations are either rejected or show larger o-a. The latter is an indication of stronger adjustments by the data assimilation for

rainy observations while the former indicates the rainy regions which are not present in the first guess.

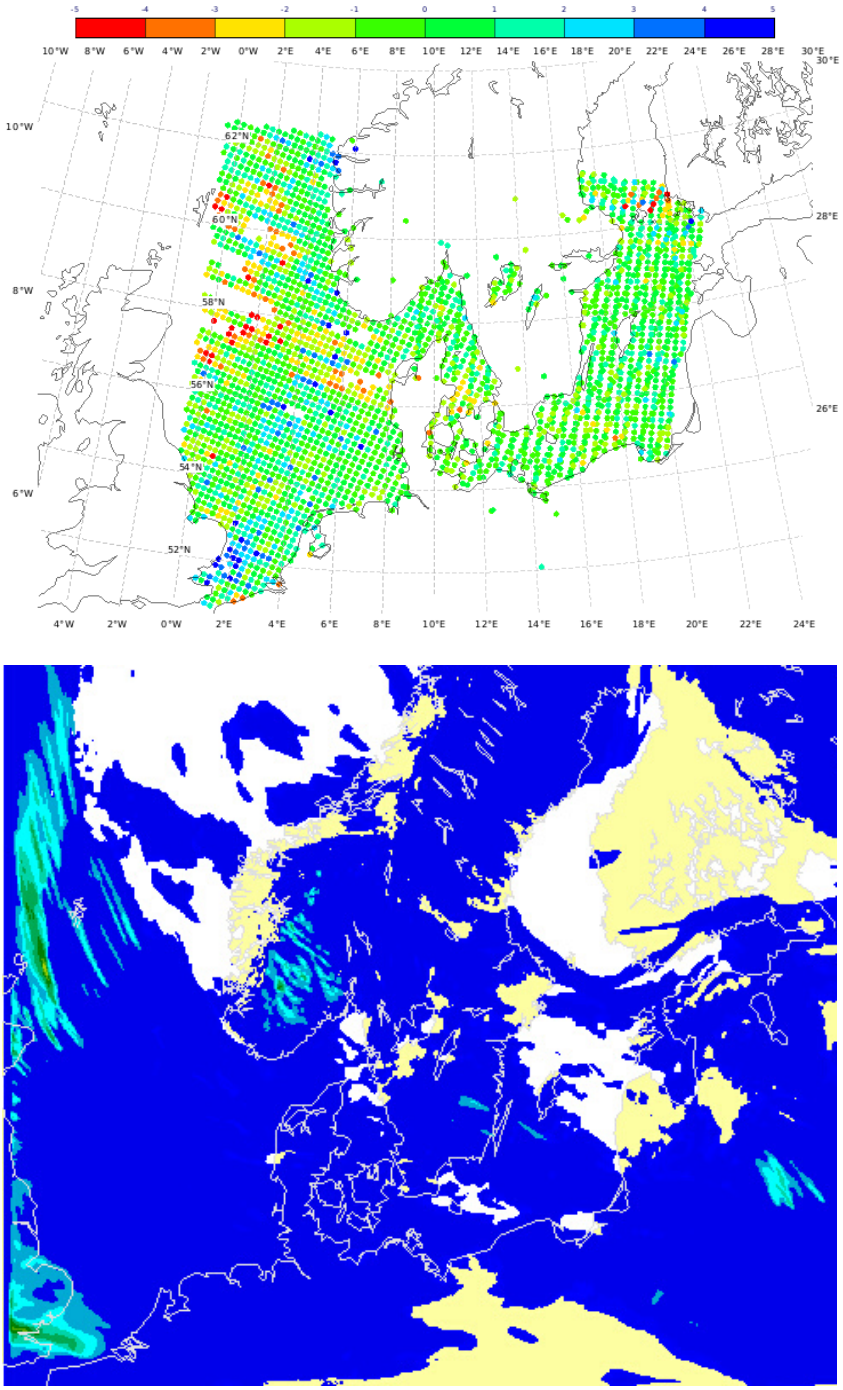

Figure 8: The o-a at 06 UTC 3rd October 2020 (top) where green dots show o-a closer to zero while the red dots show negative o-a and blue dots positive o-a. The corresponding rainy areas in the model 3h forecast (bottom) where the light blue and green regions show the weaker and strong precipitation respectively.

5.4 Emissivity check

Since we want to assimilate the all-sky radiances for the first time in the Harmonie-Arome we have decided to only assimilate them over the ocean and rejected all observations over land. Therefore, the emissivity map needs to be correctly checked. We had to solve the inconsistency in the emissivity for the all-sky which is shown in Figure 9 below.

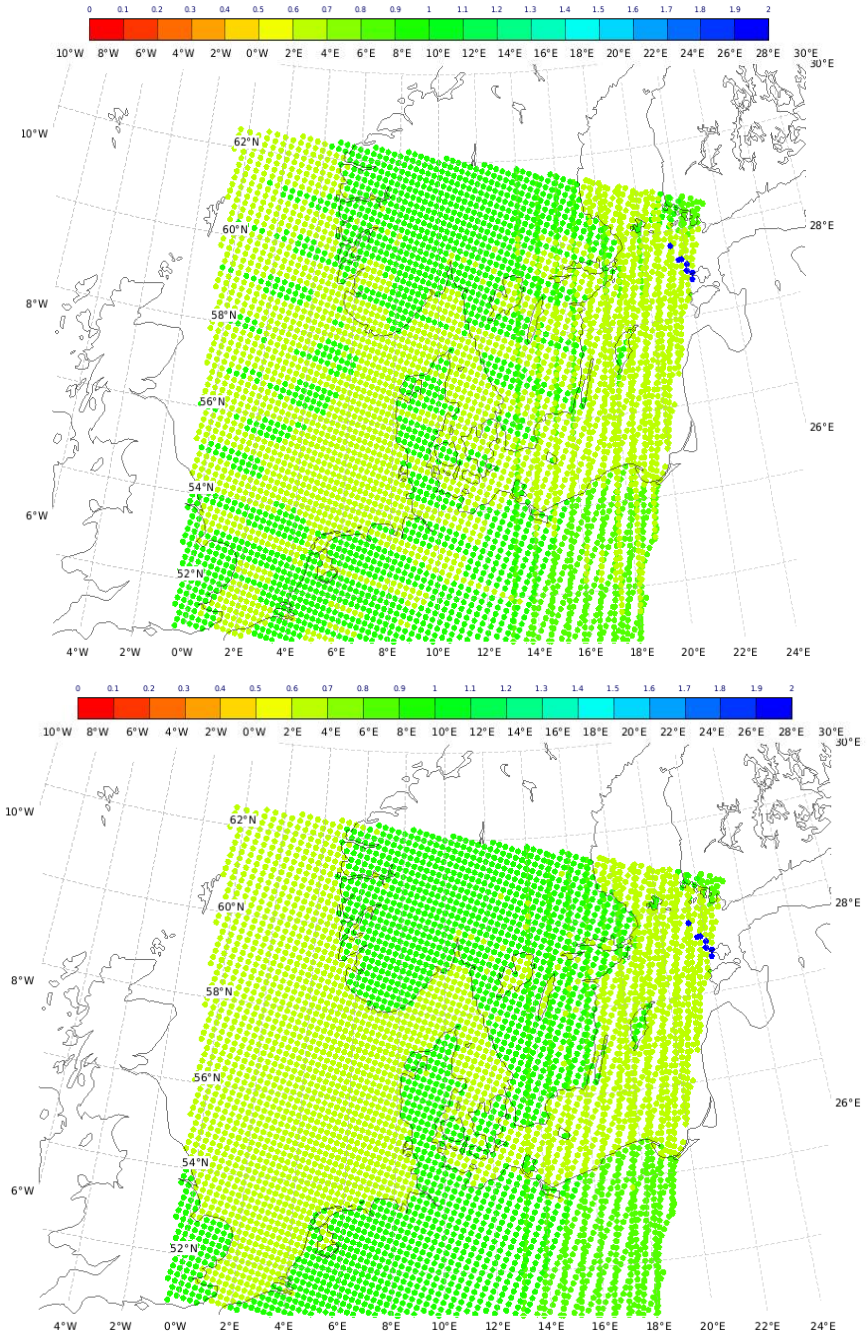

Figure 9. Emissivity maps in the first try to assimilate all-sky (upper) and clear-sky (lower) MHS observations. Note that the values are equal to 1 over land.

6 Impact study

We carried out two experiments for a one week period from 9 to 16 June 2021 over the Arome-Arctic domain. In the reference experiment only conventional observations are assimilated while in the all-sky experiment we added the assimilation of all-sky on top of conventional observations. A summary of results of this trial is described below.

6.1 Observation usage

Figure 10 shows the number of observations used in screening and minimization. The thinning method uses a coarse setup so most of the observations are removed even before the quality control stage in screening. In general, only 20-25% of observations pass the quality control in screening and the rejection is mainly due to too big first guess departures.

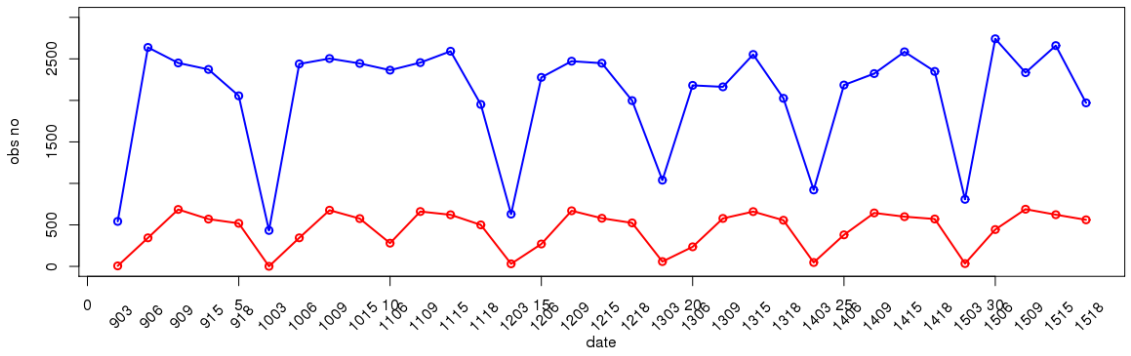

Figure 10: Time series of the number of observations before and after the quality control, i.e., in screening (blue) and minimization (red) stages.

6.2 GOM statistics

The new variables related to the hydrometeors filled under GOM structure in the all-sky assimilation are snow, rain, graupel, cloud ice, and cloud water. It should be mentioned that the graupel was not included in the version of the IFS code and was not

used in the observation operator. Also, the all-sky assimilation method requires the cloud fraction as explained in section 3. We show in Figure 11 the time series of these averaged model hydrometeors interpolated to observation locations. The magnitude of each GOM variable will directly affect the cost function and consequently the minimization process and finally the analysis itself. For the one week period in June we see that the cloud ice and snow fluxes are smallest in magnitude but cloud liquid and rain fluxes show larger values.

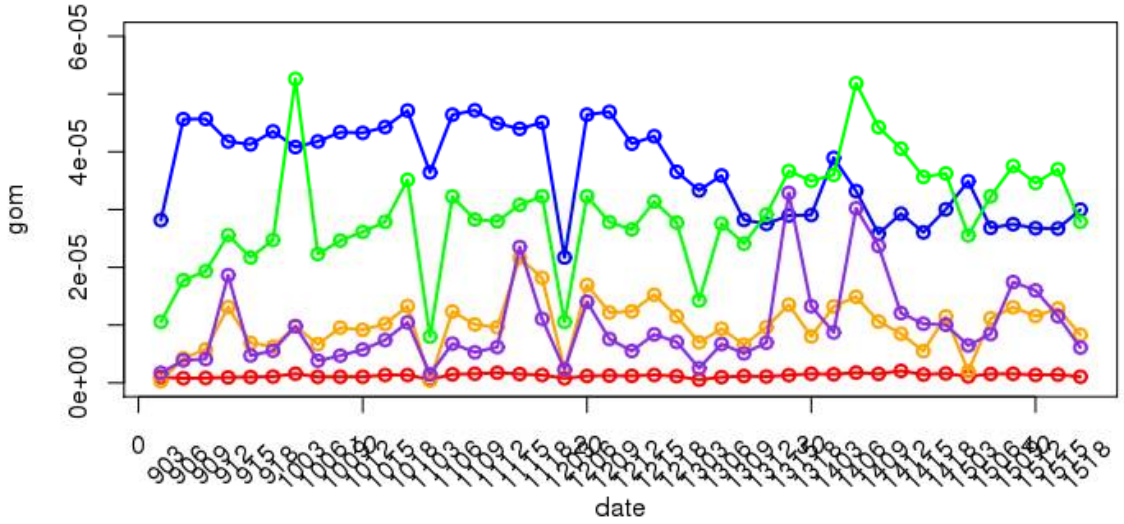

Figure 11: Time series of the GOM variables with normalised values consisting of cloud liquid (blue), cloud ice (red), rain (green), snow (orange), graupel (violet).

6.3 Brightness temperature (Tb) distribution

In this part, we examine the distribution of temperature brightness (Tb) for all observations which passed the quality control in screening and are used in the minimization. Figure 12 shows the Tb distribution for MHS channel 3. The comparison between the observation Tb against the model all-sky Tb and the model clear-sky Tb shows that there is a better correspondence between observed and all-sky Tb at lower temperature, the peak at around Tb=241 K is better represented with all-sky, and that at higher temperatures no differences is seen between all-sky and clear-sky Tb. For MHS channel 4 shown in Figure 13 the differences are more visible especially at the lower temperature even though the lower all-sky Tbs have less density than the observed one. The peaks for observed and all-sky Tb match each other both in density and the Tb value and for the higher temperatures (representing clear sky in general) no differences are found between all-sky and clear-sky Tb distributions.

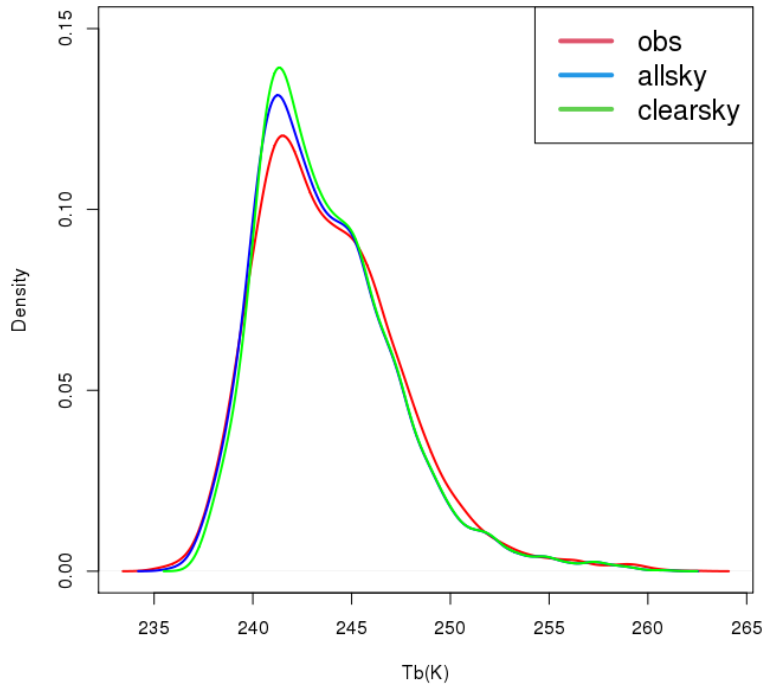

Figure 12: Observed (red), model allsku (blue), and model clear-sky (green) brightness temperature for MHS channel 3

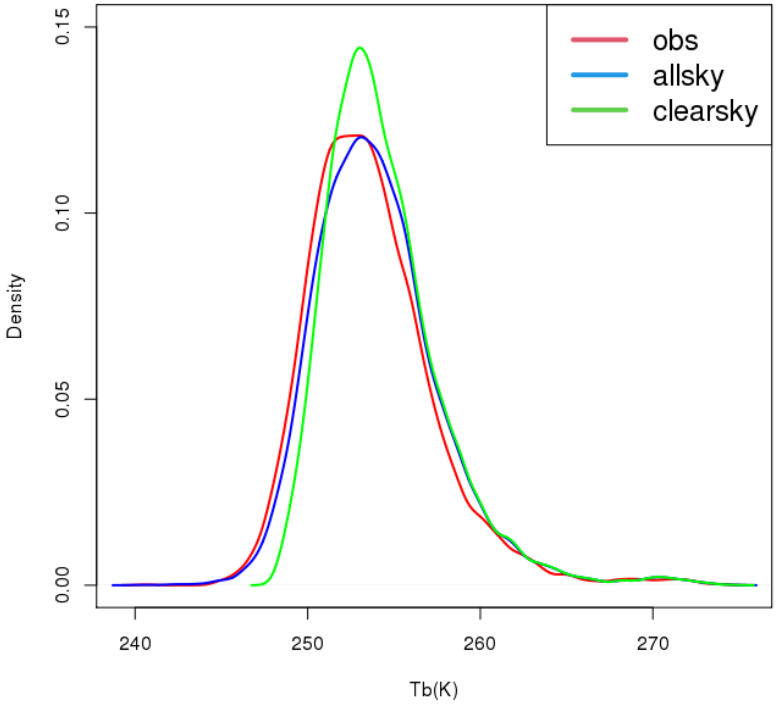

Figure 13: Observed (red), model allsky (blue), and model clear-sky (green) brightness temperature for MHS channel 4

6.4 Observation, background and analysis statistics

In the data assimilation, the calculated analysis is closer to the observations than the background to the observations, i.e., the o-a is less than o-b. Figures 14 and 15 confirm

that the all-sky assimilation is generating analysis departures smaller than the first guess departures for both channel 3 and 4. There are a few spikes in the time series but those are occurring at cycles with only a few observations. The analysis increments are shown in Figure 16 where for channel 4 there is a slightly positive bias but standard deviations are smaller than channel 3. Figure 17 shows the distribution of statistics for all-sky and for channels 3 and 4 with gaussian distributions for o-b, o-a, and a-b.

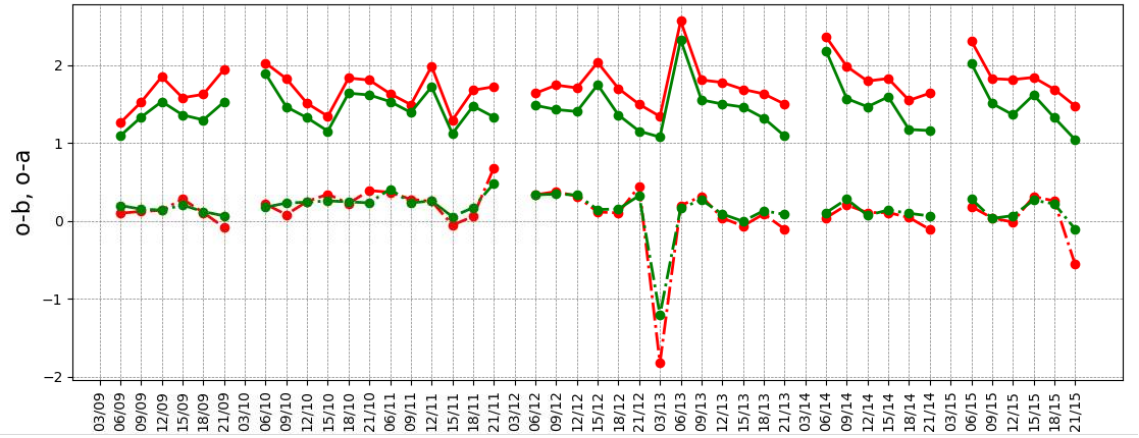

Figure 14: Mean (dashed red) and standard deviation (solid red) of observation minus background (o-b) and the mean (dashed green) and standard deviation (solid green) of observation minus analysis (o-a) for MHS channel 3 all-sky observations for a one week period.

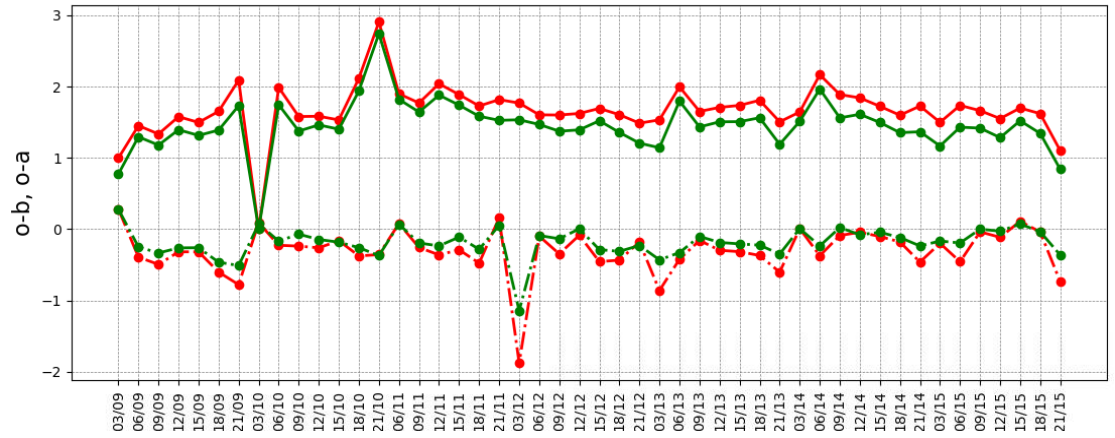

Figure 15: Mean (dashed red) and standard deviation (solid red) of observation minus background (o-b) and the mean (dashed green) and standard deviation (solid green) of observation minus analysis (o-a) for MHS channel 4 all-sky observations for a one week period.

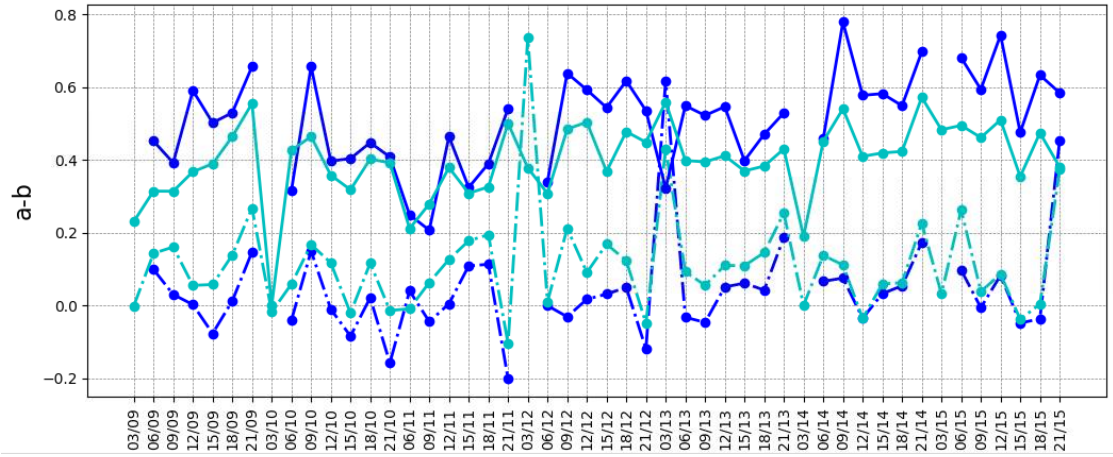

Figure 16: Mean (dashed cyan) and standard deviation (solid cyan) of analysis minus background (a-b) for MHS channel 3 all-sky and the mean (dashed blue) and standard deviation (solid blue) of observation minus analysis (o-a) for MHS channel 4 all-sky for a one week period.

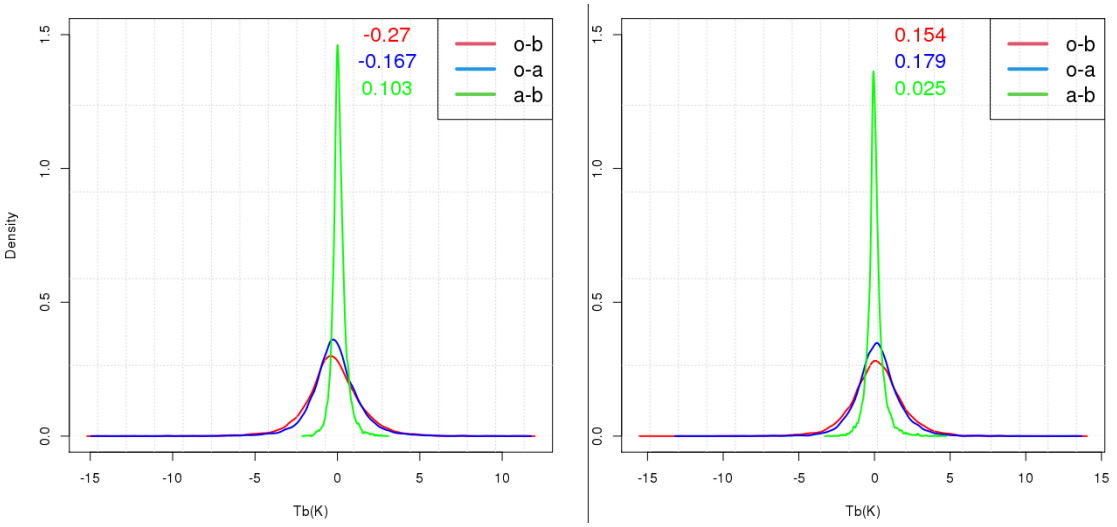

Figure 17: Distribution of observation minus background (red), observation minus analysis (blue), and analysis minus background (green) for channel 3 (right) and channel 4 (left). The numbers show the mean value for the corresponding statistics and colours.

6.5 Forecast verification

Here we verify the short range forecasts for the two experiments against the radiosonde and surface observations to find out whether the assimilation of all-sky MHS radiances improves the upper air and surface forecasts. The main feature seen in the verifications is the impact on wind where the wind speed error reduces with all-sky assimilation (*Fig. 18)*. This result is in agreement with the findings at ECMWF that all-sky assimilation is able to infer some aspects of the dynamical description of the atmosphere (*Geer et al.* 2014). Also the reduction in the bias for geopotential and dew

point observations with all-sky assimilation is interesting. The increased bias for the wind speed verification results could be related to the fact that the system should be run for a longer period so the VarBC will start to affect the results. For the surface verifications shown in Figure 19 the impact is generally neutral apart from the bias reduction for mean sea level pressure forecasts.

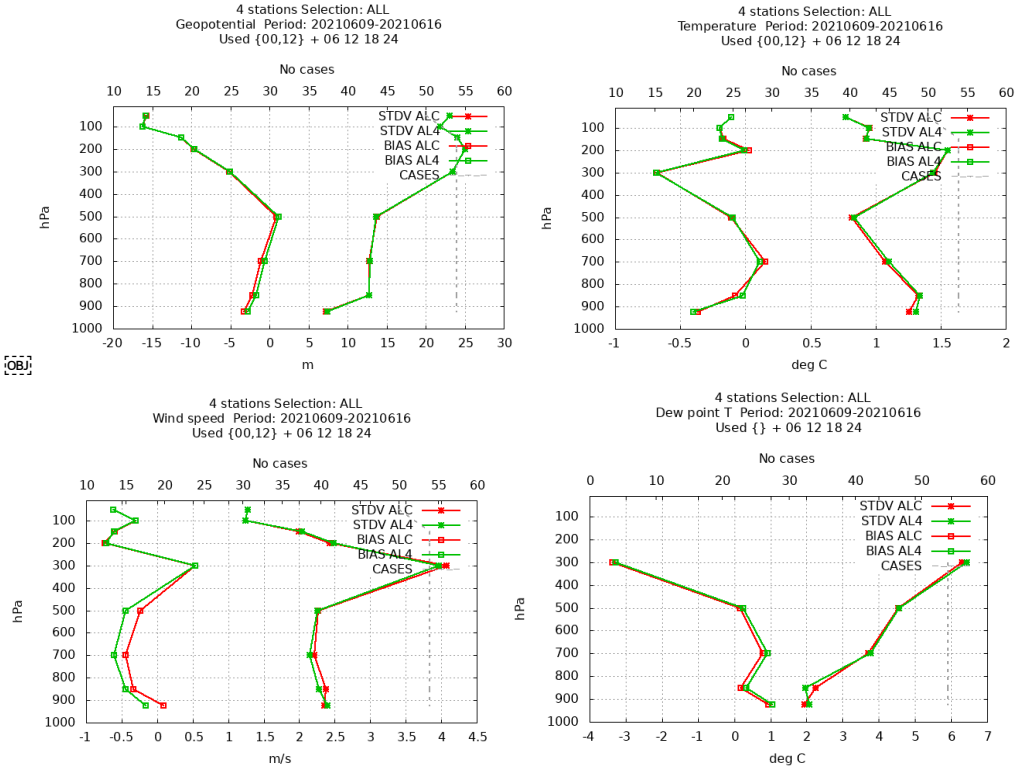

Figure 18: Forecast verification for upper air variables against radiosondes observations. The all-sky experiment is in green and the reference experiment with only conventional observations is in red.

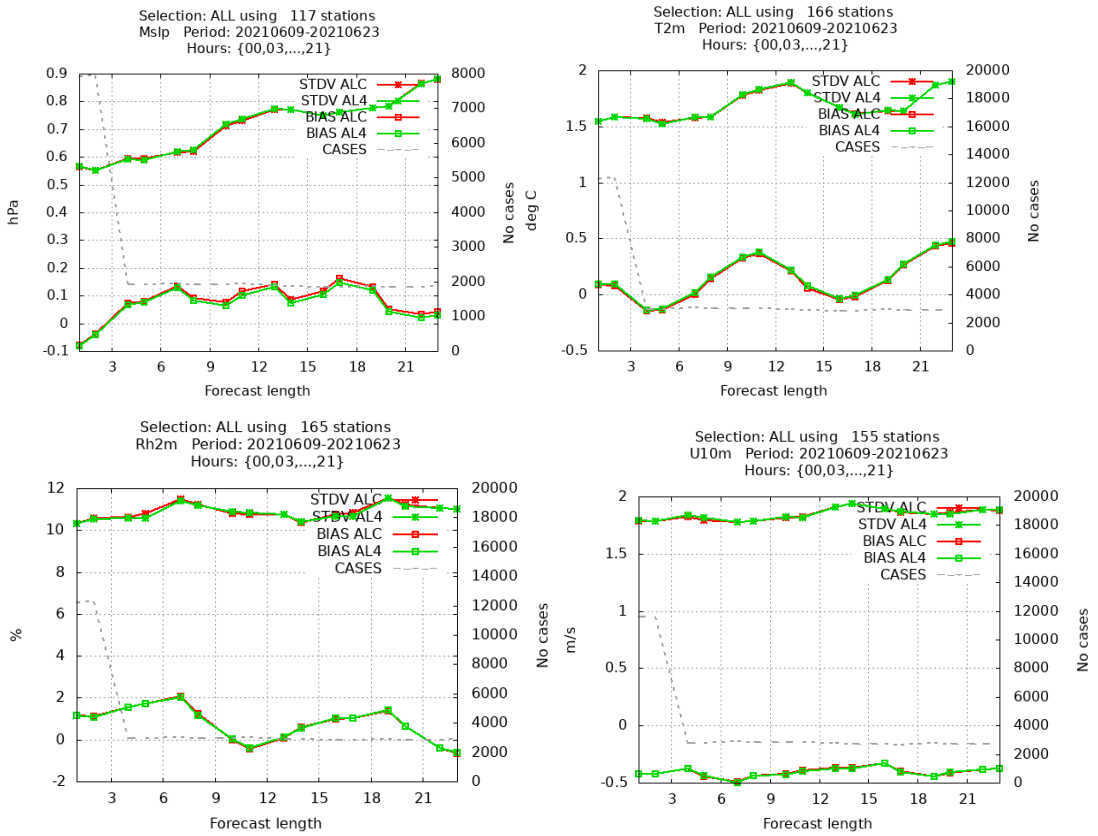

Figure 19: Forecast verification for surface variables against synoptic surface observations. The all-sky experiment is in green and the reference experiment with only conventional observations is in red.

7 Concluding remarks

The all-sky assimilation approach was not available in the Harmonie-Arome system and the implementation work done in this project had to focus mostly on the technical

issues. To introduce a completely new observation type in all parts of the assimilation system from the interface to the ODB, screening and minimization is an exhaustive task. One needs to take into account that this work was done in a version which was newly available in the Harmonie-Arome system and is not mature enough yet at the time of writing this report. However, the value of this work is to have a first image of how the all-sky assimilation works in a limited area model like Harmonie-Arome and not the least in a regional model covering the Arctic.

Our all-sky implementation shows that the Harmonie-Arome data assimilation system is capable of ingesting these new types of observations to produce well balanced model analysis fields. First, Tb distribution confirms that the all-sky low Tb values correspond better with the observations compared to the clear-sky counterparts. Secondly, the statistics confirm that for all channels the analysis increments are fairly significant although a better tuned observation error specification could change the magnitudes at certain channels and weather conditions. Another finding is that even in such a preliminary stage of the work the rainy observations are used in the data assimilation with fairly acceptable weight in the analysis calculation. Last but not the least, our one-weeks run shows that the all-sky assimilation of humidity sensitive radiances indeed has an impact on the upper air wind forecasts.

The remaining work consists of adding the graupel on top of other hydrometeor variables in the interface between the model physics and the RTTOV-SCATT operator as well as investigating the calculation and utilisation of cloud fraction from the Arome forecasts. The use of all-sky observations over land and for channel 5 also needs to be addressed. We will also perform multiple runs with non-cycled screenings to build up distribution of simulated Tbs with more samples, especially including convection cases and check the observation error values for cloudy and rainy radiances. At last, the addition of hydrometeors to the control variables will be a huge step for all-sky assimilation in the Harmonie-Arome system.

It should be mentioned that the initial results shown in this report will be part of a future publication and therefore this report should not be cited.

Acknowledgements

This study was supported by the Norwegian Research Council Project 280573 ‘Advanced models and weather prediction in the Arctic: enhanced capacity from observations and polar process representations (ALERTNESS).’ We would like to acknowledge the contributions and guidance of Philippe Chambon at Meteo-France and Alan Geer at ECMWF.

References

Auligné, T., A. P. McNally, and D. P. Dee (2007). Adaptive bias correction for satellite data in a numerical weather prediction system. Quart. J. Roy. Meteorol. Soc. 133, 631–642.

Baordo, F., A. J. Geer, and S. English (2012). SSMI/S radiances over land in the all-sky framework: one year report. EUMETSAT/ECMWF Fellowship Programme Research Report No. 27.

Bauer, P. (2001). Including a melting layer in microwave radiative transfer simulation for cloud. Atmos. Res. 57, 9–30.

Bauer, P., A. J. Geer, P. Lopez, and D. Salmond (2010). Direct 4D-Var assimilation of all-sky radiances:Part I. Implementation. Quart. J. Roy. Meteorol. Soc. 136, 1868–1885.

Bengtsson, L., and Coauthors, 2017: The Harmonie-AROME model configuration in the ALADIN-HIRLAM NWP system. *Mon. Wea. Rev.*, **145**, 1919–1935.

Berre, L., 2000: Estimation of synoptic and mesoscale forecast error covariances in a limited-area model. Mon. Wea. Rev.,128, 664−667.

Dee, D. (2004). Variational bias correction of radiance data in the ECMWF system. In ECMWF workshop proceedings: Assimilation of high spectral resolution sounders in NWP, 28 June – 1July, 2004, pp. 97–112.

Eyre, J. R. (1991). A fast radiative transfer model for satellite sounding systems. ECMWF Tech. Memo., 176, available from http://www.ecmwf.int.

Fischer, C.; Montmerle, T.; Berre, L.; Auger, L.; Stefănescu, A. An overview of the variational assimilation in the ALADIN/FRANCE NWP system. Q. J. R. Meteor. Soc. 2005, 131, 3477–3492.

Geer, A. J., P. Bauer, and C. W. O'Dell (2009). A revised cloud overlap scheme for fast microwave radiative transfer. J. App. Meteor. Clim. 48, 2257–2270.

Geer, A. J. and F. Baordo (2014). Improved scattering radiative transfer for frozen hydrometeors at microwave frequencies. Atmos. Meas. Tech. 7, 1839–1860.

Geer, A. J., Baordo, F., Bormann, N. and English, S. (2014). All-sky assimilation of microwave humidity sounders. Technical Report 741, ECMWF Tech. Memo.

Guerbette, J., Mahfouf, J.M., and Plu, M. (2016) Towards the assimilation of all-sky microwave radiances from the SAPHIR humidity sounder in a limited area NWP model over tropical regions, Tellus A: Dynamic Meteorology and Oceanography, 68:1.

Joseph, J., W. J. Wiscombe, and J. A. Weinman (1976). The delta-Eddington approximation for radiative flux transfer. J. Atmos. Sci. 33, 2452–2459.

Lawrence, H., Bormann, N., Sandu, I., Day, J., Farnan, J. and Bauer, P. (2019) Use and impact of Arctic observations in the ECMWF numerical weather prediction system. Quarterly Journal of the Royal Meteorological Society, 145, 3432–3454.

Masson, V., Moigne, P.L., Martin, E., Faroux, S., Alias, A., Alkama, R., Belamari, S., Barbu, A., Boone, A., Bouyssel, F., Brousseau, P., Brun, E., Calvet, J.-C., Carrer, D., Decharme, B., Delire, C., Donier, S., Essaouini, K., Gibelin, A.-L, Giordani, H., Habets, F., Jidane, M., Kerdraon, G., Kourzeneva, E., Lafaysse, M., Lafont, S., Lebeaupin Brossier, C., Lemonsu, A., Mahfouf, J.-F, Marguinaud, P., Mokhtari, M., Morin, S., Pigeon, G., Salgado, R., Seity, Y., Taillefer, F., Tanguy, G., Tulet, P., Vincendon, B., & Voldoire, A. (2013) The SURFEXV7.2 land and ocean surface platform for coupled or offline simulation of Earth surface variables and fluxes. Geoscientific Model Development, 6, 929–960.

McNally AP, Derber JC, Wu W, Katz BB. (2000) The use of TOVS level- 1b radiances in the NCEP SSI analysis system. Quart J Roy Meteor Soc; 126: 689-724.

Müller, M., and Coauthors, 2017: AROME-MetCoOP: A Nordic convective-scale operational weather prediction model.Wea. Forecasting, 32, 609−627.

Randriamampianina R., N. Bormann, M. A. Ø. Køltzow, H. Lawrence, I. Sandu, Z.-Q. Wang (2021): Relative impact of observations on a regional Arctic numerical weather prediction system, Q.J.R. Meteorol. Soc.

Randriamampianina, R., Schyberg, H. and Mile, M. (2019) Observing system experiments with an Arctic mesoscale numerical weather prediction model. Remote Sensing, 11, 981. (also present in SUV publications)

Saunders, R.; Hocking, J.; Turner, E.; Rayer, P.; Rundle, D.; Brunel, P.; Vidot, J.; Roquet, P.; Matricardi, M.; Geer, A.; et al. An update on the RTTOV fast radiative transfer model (currently at version 12). Geosci. Model Dev. 2018, 11, 2717–2737.

Saunders, R., J. Hocking, P. Rayer, M. Matricardi, A. Geer, N. Bormann, P. Brunel, F. Karbou, and F. Aires (2012). RTTOV-10 science and validation report. NWPSAF-MO-TV-023 v1.11, EUMETSAT NWP-SAF.

Smagorinsky, J., K. Miyakoda, and R. Strickler (1970). The relative importance of variables in initial conditions for dynamical weather prediction. Tellus 22(2), 141–157.